Seamless Transitions Between Grid-Following and Grid-Forming Control: A Novel Switching Method

Gao, Xian; Zhou, Dao; Anvari-Moghaddam, Amjad; Blaabjerg, Frede

Published in:
ICPE 2023-ECCE Asia - 11th International Conference on Power Electronics - ECCE Asia

DOI (link to publication from Publisher):
10.23919/ICPE2023-ECCEAsia54778.2023.10213821

Publication date:
2023

Document Version
Accepted author manuscript, peer reviewed version

Seamless Transitions Between the Grid-Following and the Grid-Forming Control: A Novel Switching Method

Xian Gao, Dao Zhou, Amjad Anvari-Moghaddam, and Frede Blaabjerg
AAU Energy, Aalborg University, Aalborg, DK-9220, Denmark

***Abstract*- In order to adapt to complex working environments of the power grid, the grid-connected inverters need to seamlessly switch the control strategy according to different working conditions. However, the switch may pose some sudden changes on the references of the inner control loops as well as the outer control loops like power loop or voltage loop, which results in distorted voltages and currents or even the risk of safe operation. In order to solve this problem, this paper proposes a smooth switching method between the grid-following and the grid-forming control under the grid-connected mode. A time-domain simulation model is built in Matlab/Simulink to verify the effectiveness of the proposed control method, showing it works appropriately. Finally, an experimental prototype is established to verify the effectiveness of the proposed method.**

***Index Terms*— Grid-connected inverters, smooth switching method, grid-following control, grid-forming control**

I. INTRODUCTION

With the intensification of the global energy crisis and environmental problems, distributed energy has been developed vigorously. The proportion of distributed energy in the power grid is increasing year by year. The distributed energy is usually connected to the power grid through power electronic inverters. There are normally two common control modes of the inverter [1]. One is the grid-following (GFL) control, which regulates the active and reactive power injected to the power grid and has a fast response but provides almost no inertia for the system. It is synchronized by a phase-locked loop (PLL). The other one is the grid-forming (GFM) control, which regulates the frequency and the voltages of the inverter outputs and provides inertia and damping for the system.

Because the GFL control needs an extra voltage source to provide voltage and frequency references, it cannot operate in a stand-alone mode. However, the GFM control can provide the regulation of both the voltage and frequency, which enables it to operate both in the grid-tied mode and the stand-alone mode. According to this limit of the application, many methods have been proposed for the three-phase inverters to realize the smooth transition from grid-tied mode to stand-alone mode [2]-[6]. The GFL control is applied in the grid-tied mode, while the GFM control is applied in the stand-alone mode. In [3], a compensation loop is designed and added to the excitation loop to realize the seamless transition without any external signal from the detection scheme of the islanding. Two semi-parallel control paths are proposed for the GFL mode and GFM mode respectively. The two control paths keep synchronized throughout the operation of the inverter to realize the smooth switching from the GFL control to the GFM control after the islanding. However, the synchronization process is under the standby mode, where the inverter is synchronized to the power grid without injecting any power [4]. A unified control method of the grid-connected inverters for smooth transfer to stand-alone mode is proposed in [6]. Two control loops are added to the active and reactive power control (PQ control) loop to compensate the output voltages and frequency for the stand-alone mode. These literatures only consider the transition from the grid-tied mode to the stand-alone mode. In [7], two control strategies for grid-tied-to-stand-alone and stand-alone-to-grid-tied transitions are proposed.

Most of these literatures focus on the transitions between the grid-tied mode and the stand-alone mode. However, during the gird-connected mode, transitions between the GFL and GFM control are also needed to expand the stability boundary of the power system. Furthermore, the seamless transitions under the situation that the inverters inject non-zero power to the power grid are also needed to be considered.

Based on the prior-art studies [8], it has been revealed that the GFL converter suffered from the instability in the power grid with a low short-circuit ratio (SCR), while the GFM converter suffered from the instability in the power grid with a high SCR [9], [10]. It indicates that the GFL converter could be more suitable for the stiff power grid while the GFM converter is more suitable for the weak power grid. It is noted that the power grid is considered to be weak when the generation capacity from the DC side is very large, e.g. in the conditions of strong irradiance in photovoltaic system with a certain high-power rating. In this case, the GFM control is more suitable and the GFL control needs to change to the GFM control to ensure stable operation. However, when the power grid is strong, little phase difference may lead to large active power fluctuations under the GFM control, which may induce overload of the system [11], [12]. In this case, the GFL control is more suitable and the GFM control needs to change to the GFL control. For the distributed renewable energy generation system, it may be necessary to change the control mode of grid-connected inverters in order to keep stability of the power system under different working conditions.

In order to reach good performance under different working conditions and make full use of the GFL control and the GFM control, the simplest way is to propose a smooth switching control strategy between the GFL control and the GFM control which is the aim of this paper. The main contributions of this paper can be summarized as follows. (1) Comprehensive illustrations of the mathematical models of a typical three-phase grid-connected system are given. (2) Each control loop of both the GFL and GFM control are illustrated in detail. (3) A seamless switching method is presented to realize bumpless transition between the GFL and GFM control.

The rest of the paper is organized as follows. Section II illustrates the modeling of a three-phase grid-connected system. In Section III, each control loop of both the GFL and GFM control are presented in detail, and the seamless switching method is proposed. In Section IV, a time-domain simulation model is built in Matlab/Simulink to verify the effectiveness of proposed seamless switching method. Section V provides the experimental validation. Finally, some conclusions are drawn in Section VI.

II. Modeling of a Three-Phase Grid-Connected System

The topology of a grid-connected system is shown in Fig. 1, where the system consists of a three-phase inverter , an LC filter, the grid impedance and the power grid. L_f and C_f are the inductor and the capacitor of the LC filter; Z_g is the equivalent grid impedance; u_{dc} is the dc-link voltage; u_a, u_b and u_c are the converter output voltages; u_{pcca}, u_{pccb} and u_{pccc} are the voltages at the point of common coupling (PCC); u_{ga}, u_{gb} and u_{gc} are the grid voltages; i_a, i_b and i_c are the converter output currents; i_{ga}, i_{gb} and i_{gc} are the grid currents; i_{Ca}, i_{Cb} and i_{Cc} are the capacitor currents.

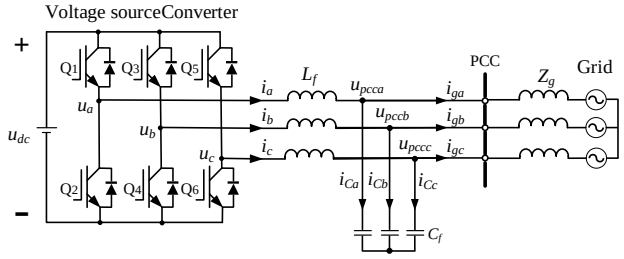

Fig. 1. Typical configuration of a grid-connected system.

Defining δ as the power angle, which is the phase angle difference between the PCC voltage vector $U_{pcc}\angle\delta$ and the grid voltage vector $U_g\angle 0$. α represents the angle of the grid impedance. The phase relationship between the PCC and the grid is shown in Fig. 2.

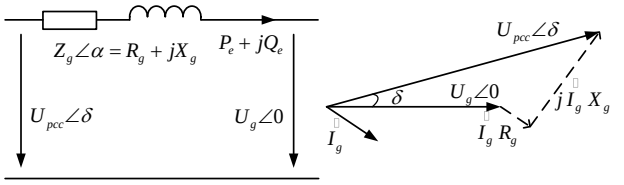

Fig. 2. Phase relationship between the PCC and the grid.

The active power p and the reactive power q flowing from the PCC to the power grid can be given as:

$$\begin{cases} p = \dfrac{3U_{pcc}^{\ 2}\cos\alpha - 3U_{pcc}U_g\cos(\alpha+\delta)}{Z_g} \\ q = \dfrac{3U_{pcc}^{\ 2}\sin\alpha - 3U_{pcc}U_g\sin(\alpha+\delta)}{Z_g} \end{cases} \tag{1}$$

In this paper, the control synchronize frame is defined by ω, which is synchronized to the voltage phase angle at the PCC. According to the Kirchhoff's voltage law, the mathematical model of the main circuit in the ω-defined rotating d-q frame can be achieved as [13], [14]:

$$u_{pccd} - u_g\cos\delta = L_g\frac{di_{od}}{dt} + R_g i_{od} - \omega L_g i_{oq} \tag{2}$$

$$u_{pccq} + u_g\sin\delta = L_g\frac{di_{oq}}{dt} + R_g i_{oq} + \omega L_g i_{od} \tag{3}$$

$$i_d - i_{od} = C_f\frac{du_{pccd}}{dt} - \omega C_f u_{pccq} \tag{4}$$

$$i_q - i_{oq} = C_f\frac{du_{pccq}}{dt} + \omega C_f u_{pccd} \tag{5}$$

$$u_d - u_{pccd} = L_f\frac{di_d}{dt} - \omega L_f i_q \tag{6}$$

$$u_q - u_{pccq} = L_f\frac{di_q}{dt} + \omega L_f i_d \tag{7}$$

where subscripts d and q represent d-axis and q-axis components of a variable, respectively.

Under the d-q frame, the expression of output active power and reactive power can be given as:

$$\begin{cases} p = \dfrac{3}{2}\left(u_{pccd}i_{od} + u_{pccq}i_{oq}\right) \\ q = \dfrac{3}{2}\left(-u_{pccd}i_{oq} + u_{pccq}i_{od}\right) \end{cases} \tag{8}$$

III. Smooth Switching Method

In this paper, the PQ control is adopted as the GFL control and the virtual synchronous generator control (VSG control) is adopted as the GFM control. The control schemes of the smooth switching method are shown in Fig. 3.

It consists of the grid synchronization loop, the power loop, the excitation loop, the voltage loop and the current loop. The grid synchronization loop can be divided into two part. The PLL unit is for the GFL control, while the power synchronization is for the GFM control. The control system is performed under the control synchronizing frame (defined by the PLL unit under the GFL control, and defined by the power synchronization loop under the GFM control), while the electrical system is performed under the actual system synchronizing frame (defined by the PCC voltage) [15]. During the steady state, the two synchronizing frames are the same. However, during the dynamic state, there is a small difference between the two synchronizing frames. In order to obtain more accurate models, this difference is taken into consideration. The variables under the control synchronizing frame are marked with the superscript c, while the variables under the actual system synchronizing frame are marked with the

superscript s.

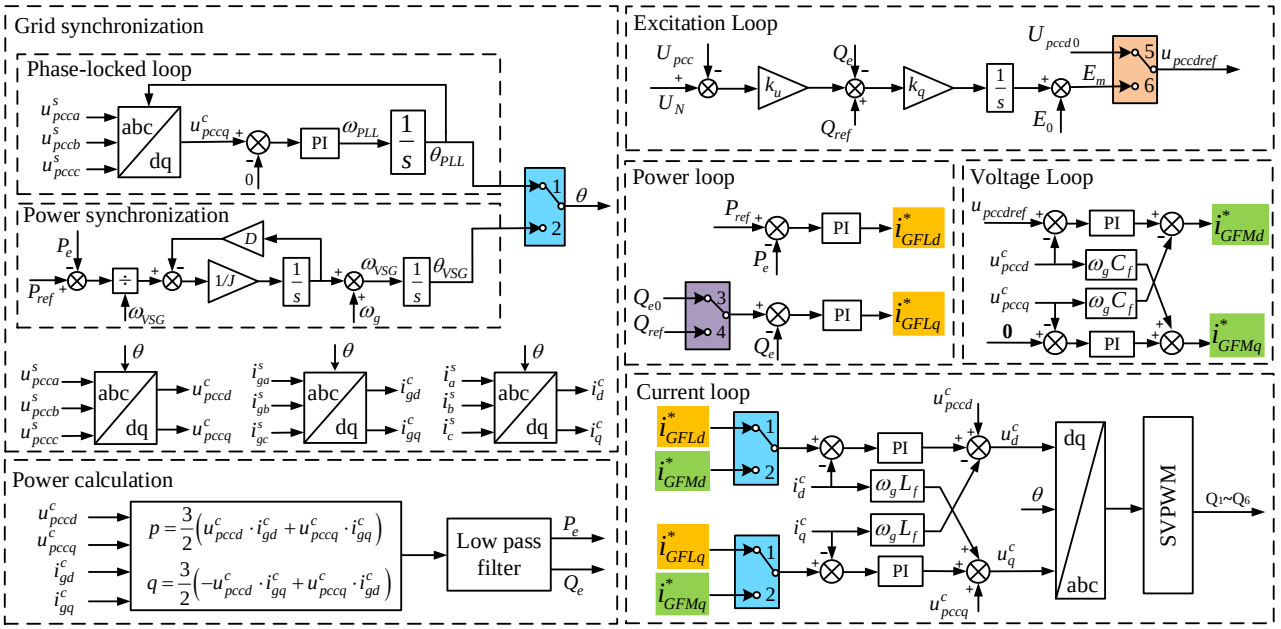

Fig. 3. Control schemes of the smooth switching method.

A. *Grid-following control*

The GFL control consists of the PLL unit, the power loop and the current loop. The GFL control adopts a PLL unit to enable the inverter synchronized to the power grid. The outer power control loop adjusts the active and reactive power injected to the power grid. The outputs of the power loop are the references for the current loop which are defined as i^*_{GFLd} and i^*_{GFLq}, respectively. The outputs of power loop can be given as follows:

$$\begin{cases} i^*_{GFLd} = \left(k_{pPQ} + k_{iPQ}/s\right)\left(P_{ref} - P_e\right) \\ i^*_{GFMq} = -\left(k_{pPQ} + k_{iPQ}/s\right)\left(Q_{ref} - Q_e\right) \end{cases} \tag{9}$$

where k_{pPQ} and k_{iPQ} are the proportional and integral coefficients of the power controller.

The inner current loop is adopted to adjust the converter currents to follow the references set by the outer power loop. The outputs of current loop can be given as follows:

$$\begin{cases} u^c_d = \left(k_{pc} + k_{ic}/s\right)\left(i^*_{GFLd} - i^c_d\right) - \omega_g L_f i^c_q + u^c_{pccd} \\ u^c_q = \left(k_{pc} + k_{ic}/s\right)\left(i^*_{GFMq} - i^c_q\right) + \omega_g L_f i^c_d + u^c_{pccq} \end{cases} \tag{10}$$

where k_{pc} and k_{ic} are the proportional and integral coefficients of the current controller; ω_g presents the grid angular frequency.

B. *Grid-forming control*

The GFM control consists of the power synchronization loop, the excitation loop, the voltage control loop and the current control loop. The GFM control does not need a PLL unit to realize the synchronization. It mimics the power synchronization characteristics of conventional synchronous generators, which is known as the swing equation. The swing equation can be given as follows:

$$\begin{cases} J\dfrac{d\omega_{VSG}}{dt} = \dfrac{P_{ref}}{\omega_{VSG}} - \dfrac{P_e}{\omega_{VSG}} - D\left(\omega_{VSG} - \omega_g\right) \\ \dfrac{d\theta_{VSG}}{dt} = \omega_{VSG} \end{cases} \tag{11}$$

where J represents the moment of inertia; D represents the damping coefficient; ω_{VSG} presents the angular frequency of the VSG control.

For the GFM control, the voltage magnitude can be estimated in the local reference frame through the excitation loop instead of a PLL unit. The excitation loop adopts the drop control with an integrator, which is also called droop-I control [16]. The excitation loop can be given as follows:

$$E_m = E_0 + k_q \int \left(k_u\left(U_N - u_{pcc}\right) + Q_{ref} - Q_e\right) \tag{12}$$

where k_q is an integral gain; k_u is the voltage droop coefficient; E_0 is the no-load electromotive force of the converter; U_N is the peak value of the rated grid voltage.

The voltage loop regulates the PCC voltages to follow the references set by the excitation loop, which can be given as follows:

$$\begin{cases} i^c_{dref} = \left(k_{pu} + k_{iu}/s\right)\left(u_{pccdref} - u^c_{pccd}\right) - \omega_g C_f u^c_{pccq} \\ i^c_{qref} = \left(k_{pu} + k_{iu}/s\right)\left(0 - u^c_{pccq}\right) + \omega_g C_f u^c_{pccd} \end{cases} \tag{13}$$

where k_{pu} and k_{iu} are the proportional and integral coefficients of the voltage controller.

The current loop of the GFM control is almost the same with that of the GFL control. The only difference is that the references of the current loop under the GFM control are determined by the voltage control, while the references of the current loop under the GFL control are determined by the outer power control. Thus, it will not be described in detail here. The references of the current loop under the GFM control are defined as i^*_{GFMd} and i^*_{GFMq}.

C. Smooth switching method between the grid-forming and grid-following control

Because both the GFL and GFM control have the same inner current loop, only the outer loop should be regulated during the switching period. In order to realize smooth transition between the GFL and GFM control, the references of the inner current loop should be the same. In addition, the steady-state operating points before and after the transition should be the same.

Because the switching is under the grid-connected mode, if the P_{ref} of the GFL and GFM control are the same, the output of the power synchronization loop ω_{VSG} is the same as that of the PLL unit ω_{PLL} during the steady-state. Thus, it is easy to realize the smooth switching in the gird synchronization part. As for switching from the GFM control to the GFL control, the grid synchronization part should be changed from the power synchronization loop to the PLL unit. The output of the integrator in the power synchronization should be set as the initial value of the integrator in the PLL unit during the transition, and the switch in the grid synchronization part is needed to switch from position '2' to '1'. As for switching from the GFL control to the GFM control, the grid synchronization part should be changed from the PLL unit to the power synchronization loop. The output of the integrator in the PLL unit should be set as the initial value of the integrator in the power synchronization during the transition, and the switch in the grid synchronization part is needed to switch from position '1' to '2'.

When changing from the GFM control to the GFL control, in order to ensure the same steady-state operation points before and after the transition, the P_{ref} and Q_{ref} of the GFL control should be the same as the P_{e0} and Q_{e0} of the GFM control under the steady-state operation. Because the converter is connected to the power grid, the frequency is equal to ω_g. The P_{ref} and P_{e0} are the same. However, as for the Q_e because of the regulation of excitation loop, there is a droop relationship between the reactive power and the voltages at the PCC during the steady-state operation, which can be expressed as:

$$k_u\left(U_N - U_{pcc}\right) + Q_{ref} - Q_e = 0 \tag{14}$$

If the PCC voltage is unequal to U_N, the Q_e under the GFM control will not track the Q_{ref}, which may lead to the difference of the steady-state operating points before and after the transition. For that, the steady-state value Q_{e0} of the GFM control should be calculated and set as Q_{ref} of the GFL control. Combining (1)-(8) and (14), the steady-state value of the output reactive power Q_{e0} can be calculated. When changing from the GFM control to the GFL control, the switch in the power control loop should be in position '3' to make sure the same operating point before and after the transition. The switch in the current control part is needed to switch from position '2' to '1'. After the switching, when the converter can well track the P_{ref} and Q_{ref}, the switch in the power control loop can switch to the position '4' to regulate the Q_e tracking the Q_{ref}.

When changing from the GFL control to the GFM control, in order to ensure the same steady-state operation points before and after the transition, the $u_{pccdref}$ and $u_{pccqref}$ of the GFM control should be the same as the U_{pccd0} and U_{pccq0} of the GFL control under the steady-state operation. Because during the steady-state, the $u_{pccqref}$ and U_{pccq0} are equal to 0, only the $u_{pccdref}$ and U_{pccd0} is needed to be considered. Combining (1)-(8), assuming P_e and Q_e can well track the references P_{ref} and Q_{ref} without any static error, U_{pccd0} can be calculated. When changing from the GFL to GFM control, the switch in the current control part switch from position '1' to '2' and the excitation loop is not activated where the switch should be in position '5'. After the switching, when the converter enters into steady state, the excitation loop is enabled and the switch should be in position '6'.

IV. Simulation Results

In order to verify the effectiveness of the proposed smooth switching method, a case study system is established in Matlab/Simulink. The key parameters of the case study are listed in TABLE I.

TABLE I

Parameters of a 1.5 kW Grid-Connected Converter

Grid Parameters		
u_g	Grid voltage	50 V
f_g	Grid frequency	50 Hz
ω_g	Grid angular frequency	314 rad/s
L_g	Grid impedance	3 mH
R_g	Grid resistance	0.18 Ω
SCR	Short-circuit ratio	5.2
Converter Parameters		
u_{dc}	DC-side voltage	600 V
L_f	Filter inductance	3 mH
C_f	Filter capacitance	20 μF
L_g	Grid inductance	3 mH
R_g	Grid resistance	0.24 Ω
P_{ref}	Rated active power	1.5 kW
Q_{ref}	Rated reactive power	0 kVar
f_s	Switching frequency	10 kHz
f_{sa}	Sampling frequency	20 kHz
Controller Parameters		
ω_{pll}	Bandwidth of phase-locked loop	13.4 rad/s
ω_{PQ}	Bandwidth of power loop	110 rad/s
ω_{vsg}	Bandwidth of VSG loop	2.77 rad/s
ω_u	Bandwidth of voltage loop	23.4 rad/s
D	Damping coefficient	9
J	Virtual inertia	0.2 kg/m^2
E_0	No-load electromotive force of the converter	70.7 V
U_N	Peak value of the rated grid voltage	70.7 V
k_u	Q-U loop coefficient	30
k_q	Integrity coefficient	0.05
ω_i	Bandwidth of current loop	1030 rad/s
ω_c	Cut-off frequency of LPF	100 rad/s

When the converter changes from the GFM control to the GFL control, the steady-state value of the reactive power Q_{e0} under the GFM control is needed to be calculated. The output reactive power of the GFM control has a droop relationship with the PCC voltage which is shown in (14). Because of the voltage control loop, the steady-state value of the q-axis component of the PCC voltage U_{pccq0} is 0, and the steady-state value of the PCC voltage U_{pcc0} is equal to its d-axis component U_{pccd0}. Based on the analysis above and the parameters shown in TABLE I, setting all the differential terms as 0 in (2)-(7) and combining (1), (8) and (14), the steady-state value of the reactive power Q_{e0} can be calculated as -25 Var.

When the converter changes from the GFL control to the GFM control, the steady-state value of the d-axis component and the q-axis component of the PCC voltage U_{pccd0} and U_{pccq0} under the GFL control are needed to be calculated. As for the GFL converter, because of the outer power control loop, the output active power P_e and reactive power Q_e are set as P_{ref} and Q_{ref}. Furthermore, because of the PLL unit, U_{pccq0} is 0. Based on the analysis above and the parameters shown in TABLE I, setting all the differential terms as 0 in (2)-(7) and combining (1) and (8), the steady-state value of the d-axis component of the PCC voltage U_{pccd0} can be calculated as 71.6 V.

When the control mode changes from the GFM to GFL control at t=2s, the waveforms of PCC voltages and converter currents without smooth switching control are shown in Fig. 4. Both the PCC voltages and converter currents have some oscillations during the switching time. The waveforms of PCC voltages and converter currents with smooth switching control are shown in Fig. 5. The GFM control mode changes to the GFL control mode at t=2s, and the reference of reactive power control changes from Q_{e0} to 0 at t=2.6s. It is evident that, with the proposed

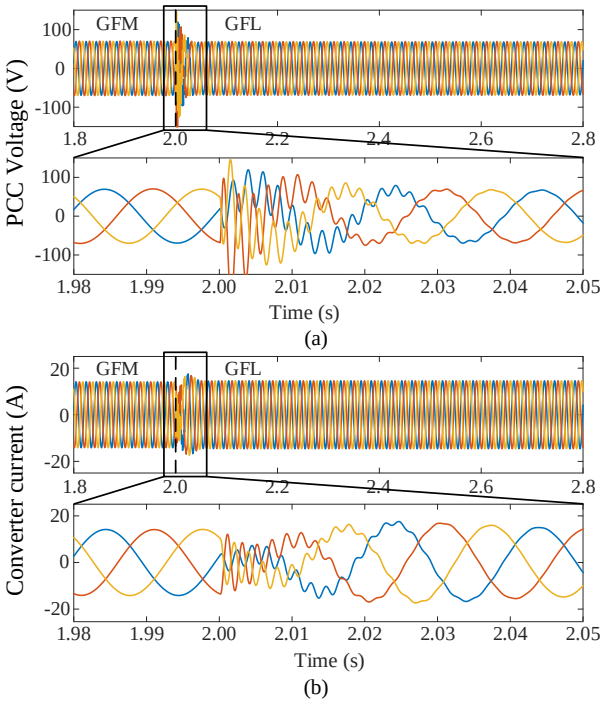

Fig. 4. Simulation of switching from grid-forming to grid-following without smooth switching control. (a) PCC voltages; (b) Converter output currents.

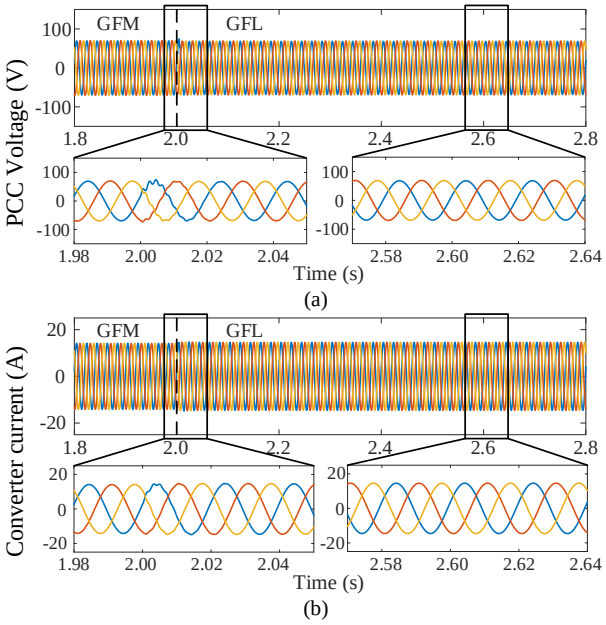

Fig. 5. Simulation of switching from grid-forming to grid-following with smooth switching control. (a) PCC voltages; (b) Converter output currents.

smooth switching control, during the switching time, both the PCC voltages and converter currents only have very slight oscillation and do not have any overshoot.

In the case of the control mode changing from the GFL to GFM control at t=2s, the waveforms of PCC voltages and converter currents without smooth switching control are shown in Fig. 6. The PCC voltages and converter currents oscillate during the switching period. The waveforms of PCC voltages and converter currents with smooth switching control are shown in Fig. 7. At t=2s, the GFL control changes to the GFM control, and the

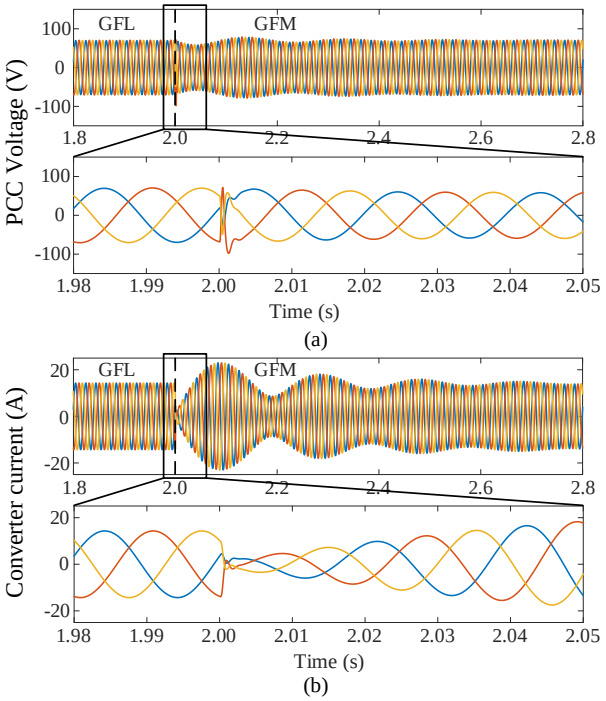

Fig. 6. Simulation of switching from grid-following to grid-forming without smooth switching control. (a) PCC voltages; (b) Converter output currents.

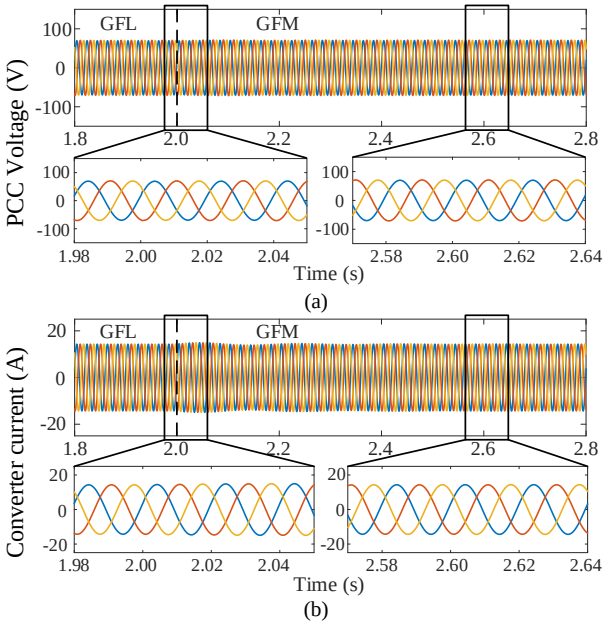

Fig. 7. Simulation of switching from grid-following to grid-forming with smooth switching control. (a) PCC voltages; (b) Converter output currents.

excitation loop is activated at t=2.6s. With the proposed smooth switching control, during the switching period, both the PCC voltages and converter currents have realized a smooth switching.

V. Experimental Validation

In order to verify the effectiveness of the proposed smooth switching method, a three-phase grid-connected system is established and the experimental setup is shown in Fig. 8. The parameters of the experimental setup are the same as those specified in TABLE I in Section IV. The three-phase grid-connected converter is based on the Imperix standard PEB-SiC-8024 module, and three high-fidelity linear amplifiers APS 15000 are used to simulated as the connected power grid. The converter currents and grid currents are measured by the LEM LAH50-P current sensors. The PCC voltages are measured by the LEM LV20-P voltage sensors. All the measured data are sent to B-BOX RCP control platform. The control algorithm is coded in a personal computer and loaded to the B-BOX RCP control platform via the patch cable. The Imperix cockpit is used to monitor and turn the control variables in real-time.

When the control mode changes from the GFM to GFL control, the experimental waveforms of PCC voltages and converter currents without the smooth switching control are shown in Fig. 9. The experimental waveforms of PCC voltages and converter currents with the smooth switching control are shown in Fig. 10. As is shown in Fig.9, during the switching time, the converter currents oscillate. When the smooth switching control is applied, both the PCC voltages and converter currents have realized a smooth switch which is shown in Fig. 10.

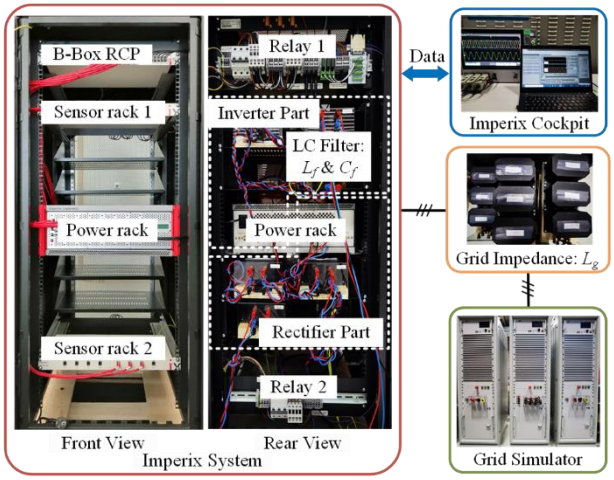

Fig. 8. Experimental setup of a three-phase grid-connected system.

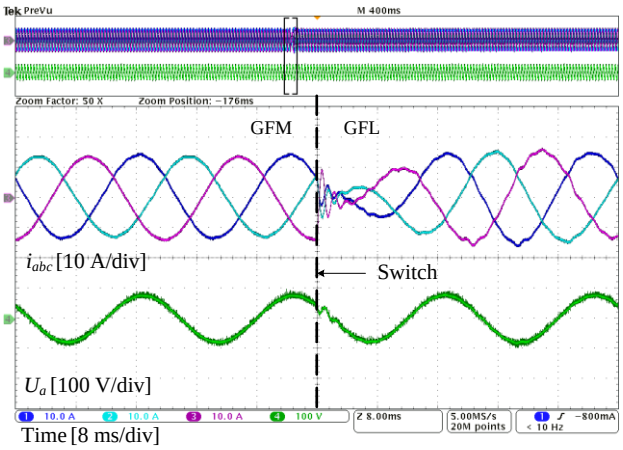

Fig. 9. Experimental waveforms of PCC voltages and converter currents changing from grid-forming to grid-following without smooth switching control.

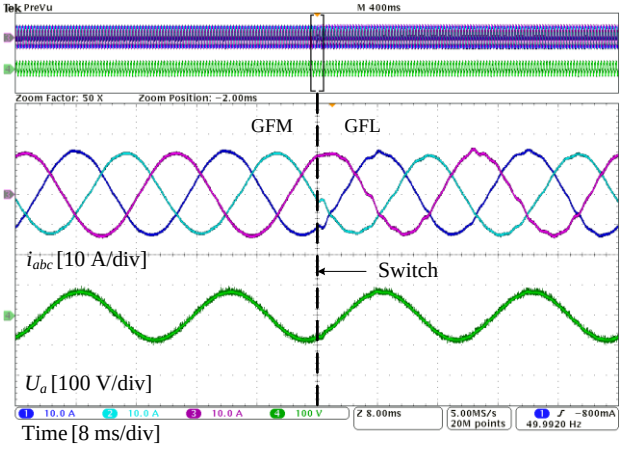

Fig. 10. Experimental waveforms of PCC voltages and converter currents changing from grid-forming to grid-following with smooth switching control.

When the control mode changes from the GFL to GFM control, the experimental waveforms are shown below. The experimental waveforms of PCC voltages and converter currents without the smooth switching control are shown in Fig. 11. The experimental waveforms of PCC voltages and converter currents with the smooth switching control are shown in Fig. 12. Comparing the dynamic performance without and with the proposed control, it is

clear that the proposed smooth switching control works well and can obviously smoother the transition between the GFL control and GFM control.

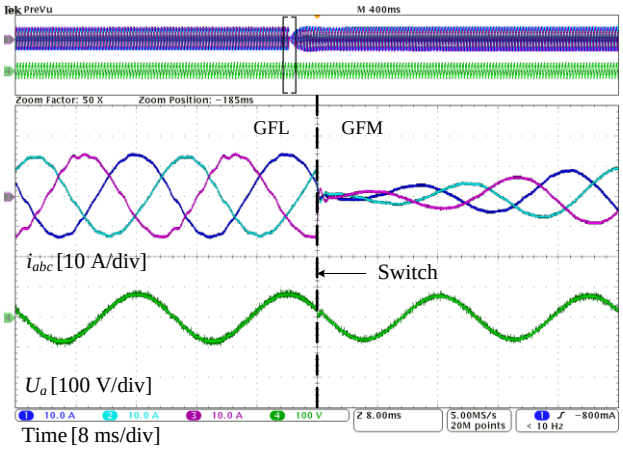

Fig. 11. Experimental waveforms of PCC voltages and converter currents changing from grid-following to grid-forming without smooth switching control.

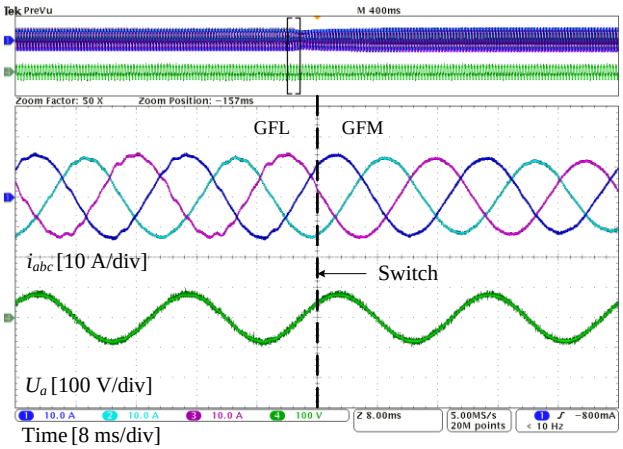

Fig. 12. Experimental waveforms of PCC voltages and converter currents changing from grid-following to grid-forming with smooth switching control.

VI. Conclusion

Since the GFL control and the GFM control are suitable for different strength levels in the power grid, a collective control design can be considered to reach good performance depending on external grid conditions. In order to realize the collective control, this paper has proposed a smooth switching method to ensure a seamless transition between the GFL control and the GFM control under the grid-connected mode. The simulation and experimental results have verified the effectiveness of the proposed method.

References

[1] J. Rocabert, A. Luna, F. Blaabjerg, and P. Rodríguez, “Control of Power Converters in AC Microgrids,” *IEEE Trans. Power Electron.*, vol. 27, no. 11, pp. 4734-4749, Nov. 2012.

[2] M. Ganjian-Aboukheili, M. Shahabi, Q. Shafiee and J. M. Guerrero, "Seamless Transition of Microgrids Operation From Grid-Connected to Islanded Mode," *IEEE Trans. Smart Grid*, vol. 11, no. 3, pp. 2106-2114, May 2020.

[3] A. B. Piardi, E. L. Geraldi, A. P. Grilo, R. Reginatto and R. A. Ramos, "A Control Structure for Smooth Transfer From Grid-Connected to Islanded Operation of Distributed Synchronous Generators," *IEEE Trans. Power Del.*, vol. 35, no. 2, pp. 929-936, April 2020.

[4] F. Sadeque and B. Mirafzal, "A Universal Controller for Grid-Forming Inverters in Microgrid during Islanding for Low Transient Current," in *Proc. 1st IEEE Int. Conf. Ind. Electron.: Developments & Appl.*, pp. 62-67, 2022.

[5] K. -Y. Lo and Y. -M. Chen, "Design of a Seamless Grid-Connected Inverter for Microgrid Applications," *IEEE Trans. Smart Grid*, vol. 11, no. 1, pp. 194-202, Jan. 2020.

[6] M. Kwon, S. Park, C. -y. Oh, J. Lee and S. Choi, "Unified Control Scheme of Grid-Connected Inverters for Autonomous and Smooth Transfer to Stand-Alone Mode," *IEEE Trans. Power Electron.*, vol. 37, no. 1, pp. 416-425, Jan. 2022.

[7] D. S. Ochs, B. Mirafzal and P. Sotoodeh, "A Method of Seamless Transitions Between Grid-Tied and Stand-Alone Modes of Operation for Utility-Interactive Three-Phase Inverters," *IEEE Trans. Ind. Appl.*, vol. 50, no. 3, pp. 1934-1941, May-June 2014.

[8] X. Gao, D. Zhou, A. Anvari-Moghaddam and F. Blaabjerg, "Stability Analysis of Grid-Following and Grid-Forming Converters Based on State-Space Model," in *Proc. 10th Int. Conf. Power Electron.* ECCE Asia, Himeji, 2022, pp. 422-428, Japan.

[9] Y. Li, Y. Gu and T. C. Green, "Revisiting Grid-Forming and Grid-Following Inverters: A Duality Theory," *IEEE Trans. Power Syst.*, vol. 37, no. 6, pp. 4541-4554, Nov. 2022.

[10] X. Wang, M. G. Taul, H. Wu, Y. Liao, F. Blaabjerg, and L. Harnefors, “Grid-Synchronization Stability of Converter-Based Resources—An Overview,” *IEEE Open J. Ind. Appl.*, vol. 1, pp. 115-134, 2020.

[11] R. H. Lasseter, Z. Chen, and D. Pattabiraman, “Grid-Forming Inverters: A Critical Asset for the Power Grid,” *IEEE J. Emerg. Sel. Top. Power Electron.*, vol. 8, no. 2, pp. 925-935, Jun. 2020.

[12] D. Pattabiraman, R. H. Lasseter, and T. M. Jahns, “Comparison of Grid Following and Grid Forming Control for a High Inverter Penetration Power System,” in *Proc. of PESGM 2018*, pp. 1-5, 2018.

[13] B. Wen, D. Boroyevich, R. Burgos, P. Mattavelli, and Z. Shen, “Analysis of D-Q Small-Signal Impedance of Grid-Tied Inverters,” *IEEE Trans. Power Electron.*, vol. 31, no. 1, pp. 675-687, Jan. 2016.

[14] G. Wu, H. Sun, X. Zhang, A. Egea-Àlvarez, B. Zhao, S. Xu, S. Wang, and X. Zhou, “Parameter design oriented analysis of the current control stability of the weak-grid-tied VSC,” *IEEE Trans. Power Del.*, vol. 36, no. 3, pp. 1458-1470, 2020.

[15] X. Gao, D. Zhou, A. Anvari-Moghaddam and F. Blaabjerg, "A Comparative Study of Grid-Following and Grid-Forming Control Schemes in Power Electronic-Based Power Systems," *Power Electronics and Drives*, vol. 8, no. 1, pp. 1-20, Jan. 2023.

[16] M. Chen, D. Zhou and F. Blaabjerg, "Voltage Control Impact on Performance of Virtual Synchronous Generator," in *Proc. 10th Int. Conf. Power Electron.* ECCE Asia, pp. 1981-1986, 2021.